Journal of Hazardous Materials 168 (2009) 13–24

Contents lists available at ScienceDirect

Journal of Hazardous Materials

journal homepage: www.elsevier.com/locate/jhazmat

# A comparison of sulfur mustard and heptane penetrating a dipalmitoylphosphatidylcholine bilayer membrane

Thomas J. Müller*, Florian Müller-Plathe

*Theoretische Physikalische Chemie, Eduard-Zintl-Institut für Anorganische und Physikalische Chemie, Technische Universität Darmstadt, Petersenstrasse 20, 64287 Darmstadt, Germany*

ARTICLE INFO

*Article history:*
Received 28 August 2008
Received in revised form 6 December 2008
Accepted 28 January 2009
Available online 25 February 2009

*Keywords:*
Sulfur mustard
Mustard gas
DPPC
Penetration
Diffusion
Molecular dynamics

ABSTRACT

In the present molecular dynamics simulations we study the chemical warfare agent sulfur mustard (bis(2-chloroethyl) sulfide) and the alkane heptane inserted into a dipalmitoylphosphatidylcholine (DPPC) bilayer, a generic model for a biological membrane. We investigate the diffusion, the orientation, the preferred positioning, and the end-to-end distance of the solutes within the membrane as well as the corresponding coupling times. We compare results of equilibrium simulations and simulation at different external forces, which drag the solutes through the membrane. These properties lead to a general comparison of the rotational and translational behaviors of the two solutes during the penetration of the membrane. We show that sulfur mustard, due to its atomic charge polarization, its bigger flexibility and its smaller molecular volume, is the faster moving molecule within the membrane. In last consequence, we show that this leads to different limits for the transport mechanism as observed in these simulations. For heptane the hindrance to penetrate into the membrane is significantly higher than for sulfur mustard. In contrast to heptane molecules, which spend the most of the time penetrating the tail groups, sulfur mustard needs more time to escape the tail group–head group interface of the membrane.



## 1. Introduction

Although French, German and British chemists were working with sulfur mustard (bis(2-chloroethyl) sulfide, CAS number 505-60-2) in the 19th century [1], the oily liquid became famous in the 20th century under the names mustard gas and yperite as a persistent chemical warfare agent which was first used by the Germans to win a tactical victory against English troops in the battle near Ypres in 1917 during World War I. The warfare agent caused many deaths but far more painful casualties for which it became famous [2]. During the 20th century sulfur mustard was used in military conflicts by many nations around the world. The most recent documented usage of sulfur mustard was in 1988 against the Kurds in Iraq. Currently several nations still have old stocks of sulfur mustard [3]. The most recent official declaration of previously unreported stockpiles was made by Libya in 2004 [1].

At room temperature sulfur mustard is a oily fluid. Due to impurities weaponized sulfur mustard is brownish (yellow to black) with a slight odour of garlic, mustard and rubber. Pure $C_4H_8C_{l2}S$ is a colorless viscous liquid with a melting point at 14 °C. Sulfur mustard is barely soluble in water while it has a high solubility in organic solvents like acetone and ether, fats and oils. [4,5] Exposure to sulfur mustard causes skin and eye injuries and can also damage the respiratory system. Since sulfur mustard is a potent alkylating agent, it causes vesication of epidermal surfaces (blisters). At high dose exposure, it is genotoxic, mutagenic and carcinogenic. This toxicity is related to the ability of sulfur mustard to spontaneously form onium compounds which react with electron rich sulfhydril (–SH) and amino ($-NH_2$) groups of proteins, nucleic acids and other tissue macromolecules [6].

The severe impact of sulfur mustard on the human health comprise the majority of the work published in peer-reviewed literature. Detection, description of poisoning effects and treatment are a major part of the contributions. Physicochemical contributions, however, are quite sparse. Recently, Shukla et al. performed quantum calculations on the reaction path of nitrogen mustard derivates on DNA [7]. While the reaction schemes for reactions within the cell have been studied in detail, there is, to our best knowledge, no study about the transport mechanisms. The dependence of the toxicity on the intake path (oral, inhalation, dermal and eye) is well known but how the molecules get into the cells, where they attack DNA, is not reported. General knowledge about the membrane penetration of sulfur mustard is also important for the decontamination process, since often emulsions or more recently microemulsions [8] are used as decontamination agents.

This work starts investigating the transport process at a basic level. To act as an alkylating agent, the molecule has to travel across several membranes to get to the DNA. Since membranes are

* Corresponding author. Tel.: +49 6151 16 5289; fax: +49 6151 16 6526.
*E-mail address:* t.mueller@theo.chemie.tu-darmstadt.de (T.J. Müller).

0304-3894/$ – see front matter © 2009 Elsevier B.V. All rights reserved.
doi:10.1016/j.jhazmat.2009.01.140

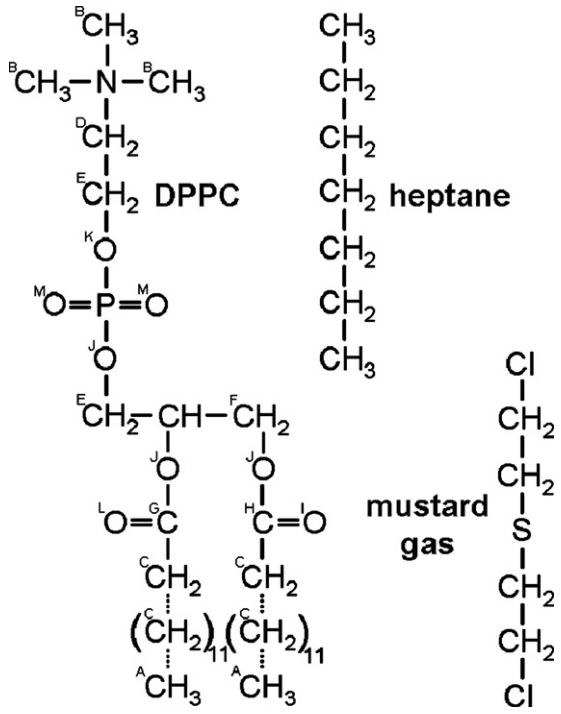


**Fig. 1.** Schematic specification and naming convention of the simulated molecules.

generally barriers to transport processes, we investigate in this computer simulation some aspects of the physicochemical behavior of sulfur mustard molecules in a model dipalmitoylphosphatidylcholine (DPPC) bilayer membrane, like their orientation, their preferred localization, and the forces required to move them. For reference, we compare these results to the structurally comparable *n*-heptane molecules in the same DPPC membrane (cf. Fig. 1).

For this type of study computer simulations, in our case molecular dynamics, provide several advantages. They are not only hazardless to execute, but also allow the necessary detailed insight into the system at the atomistic level. Computer simulations are a well established and often used method to study small molecules within membranes. Next to water, which is one of the most investigated molecules [9–11], because it is also of importance as the solvent of biological membrane systems, other relevant biological molecules like different sugars [12–14], helical structures [15], or anaesthetics [16] are topics of recent research. Computer simulations are often used to characterize the interactions between small molecules and biological membranes [17,18] and gas permeability with and without channels [19].

The present work is aimed at a qualitative understanding of the microscopic structures and processes only, as for the most part, there are no experimental values of sufficient accuracy to compare with. The understanding of motion patterns is important. A secondary goal is the investigation and elucidation of qualitative differences between the semi-hydrophobic sulfur mustard, which contains a few hetero atoms and the completely hydrophobic *n*-heptane. Using a united atoms approach for this study both molecules consist of seven atoms and are also comparable in size. But the force field description of the two molecules differ significantly in their partial charges (which sulfur mustard has and heptane has not). As we are at present not after quantitative transport coefficients, we use off-the-shelf force field parameters without further optimization, which are deemed good enough for both objectives.

## 2. Method

The simulation package which was chosen for this investigation is YASP, which was initially written by Müller-Plathe [20] and has recently been parallelized by Tarmyshov and Müller-Plathe [21].

The motion of the atoms in this program is based on a potential built of six different parts [22]:

$$V_{\mathrm{tot}} = V_{\mathrm{LJ}} + V_{\mathrm{Coulomb}} + V_{\mathrm{angle}} + V_{\mathrm{torsion}} + V_{\mathrm{hd}} + (V_{\mathrm{bond}}) \tag{1}$$

the non-bonded potentials were based on Lennard–Jones interaction $V_{\mathrm{LJ}}$ (applying the Lorentz-Berthelot mixing rules [23]) and the Coulomb interaction of partial charges $V_{\mathrm{Coulomb}}$. The truncation error induced by using a cutoff radius was reduced applying a reaction field correction. Of the bonded potentials we used the harmonic angle potential $V_{\mathrm{angle}}$, the harmonic dihedrals potential $V_{\mathrm{hd}}$, and the cosine based torsion potential $V_{\mathrm{torsion}}$ while we did not use the harmonic bond potential but fixed the distances between bonded atoms using the SHAKE algorithm [24].

To change from simulations at constant number of particles, constant volume and constant energy (NVE) to simulations at constant temperature (NVT) a Berendsen thermostat was applied to couple the system temperature to an external bath. To perform simulations at constant pressure (NPT) instead of constant volume we use additionally a Berendsen manostat [25].

In addition to equilibrium simulations, YASP also allows the user to apply constant external forces $F$ to selected atoms. This method has previously been applied to study the gas sorption and transport of small gas molecules in polyisobutylene [26]. Here it is applied to study the transport of heptane and sulfur mustard in an inhomogeneous system. The external forces are balanced in a way to conserve the total linear momentum and to avoid a drift of the system. The system responds with a flux of molecules $J$ (which depends on the simulation box volume $V$, and the velocity of the particles $v_i$) to the applied external force (here applied in the $z$ direction). From this flux the diffusion coefficient $D$ can be calculated, knowing the Boltzmann constant $k_{\mathrm{B}}$, the number density $\rho$ of the penetrant molecules, the temperature $T$, and the external force $F_z$ [22,27]:

$$J = \frac{1}{V}\sum_i (-1)^i v_i \tag{2}$$

$$D_{zz} = \frac{k_{\mathrm{B}}T}{\rho F_z}\langle J(t \to \infty)\rangle \tag{3}$$

This description will be compared to the diffusion coefficient calculated from the mean square displacement in equilibrium simulations using the Einstein relation:

$$D = \frac{1}{2\mathrm{dim}}\lim_{t\to\infty}\frac{d}{dt}\langle|\mathbf{r}(t) - \mathbf{r}(0)|^2\rangle \tag{4}$$

In this expression $t$ is the time, $\mathbf{r}$ are the coordinates of the atoms and, when treating small molecules, the molecule's center of mass. Finally, dim is the number of spatial dimension accessible to the diffusing particle. While in homogeneous bulk the particle can diffuse in all three dimensions (dim = 3), it is inhibited in a bilayer to wander in the $z$ direction (dim = 2).

We are looking at three different properties of the solutes in this paper: the position of a molecule, which was always characterized by the central atom (S in sulfur mustard, and $CH_2$ at position 4 in heptane), the end-to-end distance (ee), and the angle of the molecule to the $z$ axis (the axis perpendicular to the membrane), which is calculated from the end-to-end vector and the $z$ axis. For calculating distributions, the first two properties do not need any further modification. The orientation angle to the axis is different, since projecting the total orientation onto the $z$ axis neglects the orientation in $x$ and $y$ directions. There are more possible orientations perpendicular to the $z$ axis, than along it. To correct this effect of the

**Table 1**
Parameterization of the DPPC membrane.

| Atom/group | Code[a] | Mass $m$ [g mol$^{-1}$][b] | LJ epsilon $\varepsilon$ [kJ mol$^{-1}$][b] | LJ sigma $\sigma$ [nm][b] | Charge $q$ [e][b] |
|---|---|---|---|---|---|
| $CH_3$ | A | 15.035 | 0.8672 | 0.3748 | 0 |
| | B | 15.035 | 0.8672 | 0.3748 | 0.4 |
| $CH_2$ | C | 14.027 | 0.4105 | 0.407 | 0 |
| | D | 14.027 | 0.4105 | 0.407 | 0.3 |
| | E | 14.027 | 0.4105 | 0.407 | 0.4 |
| | F | 14.027 | 0.4105 | 0.407 | 0.5 |
| CH | | 13.019 | 0.09489 | 0.5019 | 0.3 |
| C | G | 12.011 | 0.4059 | 0.3361 | 0.7 |
| | H | 12.011 | 0.4059 | 0.3361 | 0.8 |
| N | | 14.0067 | 0.8768 | 0.2976 | −0.5 |
| P | | 30.9738 | 2.4467 | 0.3386 | 1.7 |
| O | I | 15.9994 | 1.1011 | 0.2871 | −0.6 |
| | J | 15.9994 | 1.1011 | 0.2871 | −0.7 |
| | K | 15.9994 | 1.1011 | 0.2871 | −0.8 |
| | L | 15.9994 | 1.725 | 0.2626 | −0.7 |
| | M | 15.9994 | 1.725 | 0.2626 | −0.8 |

| Bond[c] | Bond length $b$ [nm] | Torsion | Multiplicity | Phase shift $\tau$ [°] | $k_{torsion}$ [kJ mol$^{-1}$] |
|---|---|---|---|---|---|
| $CH_x$–N[d] | 0.147 | $CH_2$–$CH_2$–$CH_2$–$CH_x$[d] | 3 | 0 | 11.84 |
| $CH_2$–$CH_x$[d] | 0.153 | C–$CH_2$–$CH_2$–$CH_2$ | 3 | 0 | 11.84 |
| $CH_x$–O[d] | 0.143 | $CH_3$–N–$CH_2$–$CH_2$ | 3 | 0 | 7.54 |
| P–O | 0.161 | N–$CH_2$–$CH_2$–O | 3 | 0 | 11.72 |
| P═O | 0.148 | $CH_x$–$CH_2$–O–P[d] | 3 | 0 | 7.54 |
| C–O | 0.133 | $CH_2$–O–P–O | 3 | 0 | 2.1 |
| C═O | 0.123 | O–$CH_2$–CH–$CH_2$ | 3 | 0 | 11.84 |
| C–$CH_2$ | 0.148 | C–O–C–$CH_2$ | 2 | 180 | 33.4 |
| | | $CH_x$–$CH_x$–O–C[d] | 3 | 0 | 7.54 |
| | | O–C–$CH_2$–$CH_2$ | 6 | 0 | 2 |

| Angle | Angle $\alpha$ [°] | $k_{angle}$ [kJ mol$^{-1}$ rad$^{-2}$] | Harmonic dihedral | Phase shift $\tau$ [[°]] | $k_{dih}$ [kJ mol$^{-1}$ rad$^{-2}$] |
|---|---|---|---|---|---|
| $CH_2$–N–$CH_2$ | 109.5 | 420 | O–C–O(I,L)–$CH_2$ | 0 | 0.51 |
| Y–$CH_2$–$CH_2$[e] | 111 | 530 | | | |
| $CH_2$–O–P | 120 | 530 | | | |
| O–C–$CH_2$ | 113 | 545 | | | |
| O═C–$CH_2$ | 125 | 750 | | | |
| O–C═O | 122 | 700 | | | |
| $CH_x$–O–C[d] | 117 | 635 | | | |
| $CH_2$–CH–O,$CH_2$ | 109.5 | 520 | | | |
| O–P═O | 109.6 | 450 | | | |
| O–P–O | 103 | 420 | | | |
| O═P═O | 120 | 780 | | | |

[a] Different parameterization of the same atom/atom groups at different positions corresponding to Fig. 1.
[b] For non-bonded interactions first, second, and third neighbor interactions have set to 0.
[c] All bonds have been constrained to their average value using the SHAKE algorithm with a maximum allowed number of 500 cycles and a tolerance of $10^{-6}$.
[d] $CH_x$ is CH, $CH_2$, or $CH_3$.
[e] Y is N, C, $CH_2$ or O.

metric, the net orientation is divided by the sine of the orientation angle.

To quantify the molecular dynamical behavior of the solutes (angles to the $z$ axis, end-to-end distances (the length of the end-to-end vector), and the $z$ coordinate of the molecules, which defines their position along the membrane normal), the autocorrelation functions $A(t)$ for these properties have been evaluated:

$$A(t) = \frac{\langle (a(0) - \langle a \rangle)(a(t) - \langle a \rangle) \rangle}{(\sigma(a))^2} \quad (5)$$

In this notation $a$ symbolizes the quantity in question, $a(t)$ the specific value of this quantity at time $t$ and $\sigma$ its variance. The autocorrelation functions have been least-squares fitted to an exponential:

$$A(t) = e^{-t/\tau_{corr}} \quad (6)$$

The fitting parameters $\tau_{corr}$ are reported as the corresponding correlation times.

## 3. Computational details

### 3.1. Force fields

Since the goal of this work is not to calculate hard numbers, but to see tendencies and principles as a first step to understand the transport of sulfur mustard-like molecules, we forwent a new parameterization of a new lipid force field and translated the existing united atom bilayer force field GROMOS96 45A3 A [28] into the YASP functional form. This leads to the parameters reported in Table 1.

The definition of the potentials in GROMOS and in YASP is similar, so that we expected the behavior of our membrane to be comparable to the GROMOS one. Nevertheless there are two differences. While the GROMOS implementation works with flexible bonds the YASP adoption works with constrained bonds which where fixed to their average value using the SHAKE algorithm. The calculation of the electrostatic interactions in YASP uses a single atomic cutoff plus a reaction-field

**Table 2**
Force field parameters of sulfur mustard and heptane.

| | *n*-Heptane | Sulfur mustard |
|---|---|---|
| Mass [g mol$^{-1}$] | $m_{CH_3} = 15.023475$<br>$m_{CH_2} = 14.01565$ | $m_{Cl} = 35.453$<br>$m_{CH_2} = 14.01565$<br>$m_S = 32.06$ |
| $\varepsilon$ [kJ mol$^{-1}$][a] | $\varepsilon_{CH_3} = 0.914$<br>$\varepsilon_{CH_2} = 0.54$ | $\varepsilon_{Cl} = 1.25556$<br>$\varepsilon_{CH_2} = 0.40587$<br>$\varepsilon_S = 1.90587$ |
| $\sigma$ [nm][a] | $\sigma_{CH_3} = 0.391$<br>$\sigma_{CH_2} = 0.393$ | $\sigma_{Cl} = 0.346982$<br>$\sigma_{CH_2} = 0.33611$<br>$\sigma_S = 0.3330768$ |
| Partial charge [e][a] | $q_{CH_3} = 0$<br>$q_{CH_2} = 0$ | $q_{Cl} = -0.174487$<br>$q_{CH_2} = 0.140655$[b]<br>$q_{CH_2} = 0.164474$[c]<br>$q_S = -0.261284$ |
| Bond length [nm] | $b_{CH_x-CH_x} = 0.153$[d] | $b_{Cl-CH_2} = 0.1767$<br>$b_{CH_2-CH_2} = 0.1541$<br>$b_{CH_2-S} = 0.181$ |
| Angle [°] | $\alpha_{CH_x-CH_x-CH_x} = 109.47$[d] | $\alpha_{CH_x-CH_x-CH_x} = 109.47$ |
| $k_{angle}$ [kJ mol$^{-1}$ rad$^{-2}$] | $k_{CH_x-CH_x-CH_x} = 520$[d] | $k_{Cl-CH_2-CH_2} = 484$<br>$k_{CH_2-CH_2-S} = 545$<br>$k_{CH_2-S-CH_2} = 475$ |
| $k_{torsion}$ [kJ mol$^{-1}$ rad$^{-2}$][e] | $k_{CH_x-CH_2-CH_2-CH_2} = 11$[d]<br>$m = 1, \tau = 0$ | $k_{Cl-CH_2-CH_2-S} = 5.92$<br>$m = 1, \tau = 180$ |
| | $k_{CH_x-CH_2-CH_2-CH_2} = 6.5$[d]<br>$m = 2, \tau = 0$ | $k_{CH_2-CH_2-S-CH_2} = 5.92$<br>$m = 1, \tau = 180$ |
| | $k_{CH_x-CH_2-CH_2-CH_2} = 9.6$[d]<br>$m = 3, \tau = 0$ | |

[a] Intramolecular 1–2, 1–3 and 1–4 interactions have been omitted totally.
[b] $CH_2$ next to the chlorine atom (at positions 2 and 6).
[c] $CH_2$ next to the sulfur atom (at positions 3 and 5).
[d] $CH_x$ may be $CH_2$ or $CH_3$.
[e] In order to reduce any ambiguous influences, which do not come from the non-bonded forces, in the non-equilibrium part of this study, all torsions have been reduced to zero.

correction instead of charge groups which GROMOS takes into account.

The parameterization of the united atom force field for sulfur mustard (Table 2) was derived from several sources. The non-bonded Lennard–Jones interactions were transferred form the GROMOS96 force field [29], while bond lengths between atoms were taken from the CRC handbook [30]. The point charges on the atoms have been derived using a density-functional calculation (B3LYP) executed with the Gaussian 03 program version B.01 [31] using a 6-311G(2d,2p) basis set. In order to estimate average partial charges for the parameterization of the sulfur mustard force field we averaged the atomic partial charges derived by the built in CHELP algorithm of the all-trans conformation and of the gauche conformation of the 2–3 bond of the molecule. The geometry of the molecule was defined by the average values for bonds and angles derived above. To change form an all atom model to the united atoms model we included the charges of aliphatic hydrogen atoms into their parent carbons. The equilibrium bond angles and the associated force constants for angular vibration were again transferred from GROMOS96 [29].

### 3.2. Simulation setup

For this study, several equilibrium and non-equilibrium simulations have been performed. This section deals first with the setup of the equilibrium simulations, followed by the setup of the non-equilibrium simulations.

#### 3.2.1. Pure sulfur mustard

900 sulfur mustard molecules have been equally distributed on a grid in a cubic box with a side length of 7.741 nm. The equilibration was performed with a cutoff of 0.8 nm, a neighbor list with a cutoff of 1.0 nm which was updated every 15 time steps, and a time step of 2 fs. The simulation was performed at constant NVT conditions enforced using a Berendsen thermostat with a target temperature of $T_{targ} = 300$ K and a temperature coupling time of $\tau_T = 0.2$ ps. After 10,000 time steps, the temperature already reached the target temperature and fluctuated during the next 10,000 time steps with a standard deviation of 3 K. Switching to constant pressure (NpT) simulations using a Berendsen manostat with a target pressure $p_{targ} = 101.3$ kPa and a pressure coupling time of $\tau_p = 3$ ps was followed by another equilibration of 10,000 time steps. The subsequent production ran with a less pressure-constrained system (in order to avoid artifacts from too small coupling constants $\tau_p$ was set to 5 ps in the production runs of all systems) for a total time of 6 ns while writing out trajectory data every 1 ps.

#### 3.2.2. Pure heptane

400 molecules were equally distributed on a grid in a cubic box with side length 7.741 nm. The equilibration was also first performed for 10,000 time steps using a constant volume, constant temperature simulation ($T_{targ} = 300$ K, $\tau_T = 0.2$ ps) with a cutoff of 0.8 nm, a neighbor list with a cutoff of 1.0 nm which was updated every 15 time steps, a time step of 2 fs. Another equilibration simulation for 10,000 time steps at constant temperature and pressure ($p_{targ} = 101.3$ kPa and $\tau_p = 1.5$ ps) was finally followed by the evaluation simulation which was performed for 6 ns keeping the same parameter setup except the pressure coupling constant which was increased to $\tau_p = 5$ ps. Every 1 ps, coordinates, velocities, and intermediately evaluated values were written into files.

#### 3.2.3. Sulfur mustard and heptane in water

The initial startup configuration for these simulations was an equilibrated water box consisting of 1500 extended simple point charge (SPC/E) [32] water molecules. We introduced one heptane molecule into this box and equilibrated it using a cutoff of 1.2 nm, a neighbor list with a cutoff of 1.4 nm and an update frequency of every 5 time steps. The reaction field dielectric constant was set to 72 (the value for water). Temperature was controlled by a Berendsen thermostat ($T_{targ} = 325$ K, $\tau_T = 0.2$ ps) and pressure by a Berendsen manostat with $p_{targ} = 101.3$ kPa and $\tau_p = 1.0$ ps. Spurious drift was removed from the system every 1000 time steps, while the trajectories and calculated data were written out every 1 ps for sulfur mustard and every 0.4 ps for heptane. Using a time step of 2 fs, the equilibration was performed for 1 ns guaranteeing a constant total energy and a constant density.

Switching the force field parameters of the heptane molecule to those of sulfur mustard and performing another equilibration with the same parameters just mentioned led to the starting coordinates for the water/sulfur mustard system.

The production runs for both systems were performed with the same parameterization as in the equilibration. They ran for a total simulation time of 15 ns.

#### 3.2.4. DPPC bilayer

The bilayer was constructed from two DPPC monolayers and 3655 SPC/E water molecules. A monolayer was built from 64 all-trans DPPC molecules arranged on an equally spaced $8 \times 8$ grid (molecules oriented perpendicular to the *xy* plane) with total side length $l = 6.25$ nm. To produce the starting box, the two layers were positioned tail against tail and the cuboid box was filled with 3655 SPC/E water molecules. They were again put on a grid, so that the dimension of the whole box became 6.25 nm $\times$ 6.25 nm $\times$ 8.74 nm. This structure was first relaxed with several very short

simulations (1000 time steps) at constant volume and constant energy: The initial temperature was 325 K, the cutoff was 0.8 nm using a reaction field dielectric $\varepsilon = 54$ [28], the neighbor list cutoff was 1.0 nm, and the neighbor list was updated every 15 time steps. The time step was stepwise increased from $10^{-13}$ to $10^{-4}$ ps. After each run, the velocities of the atoms were reinitialized for the next run from a Boltzmann distribution at the target temperature. This procedure was repeated with a time step of 0.2 fs including the Berendsen thermostat with $T_{\text{targ}} = 325$ K and $\tau_T = 0.2$ ps until the temperature sank below 400 K. The temperature relaxation was finished with a simulation of 10,000 time steps with a time step of 2 fs. Then the system was shifted to constant pressure calculations additionally using independent Berendsen pressure coupling for each Cartesian direction (compressibility $\kappa = 2.77 \times 10^{-7}$ kPa$^{-1}$). In a first run of 1000 time steps of 2 fs, the system was forced to compact in $z$ direction ($p_{x,\text{targ}} = p_{y,\text{targ}} = 101.3$ kPa with $\tau_{p,x} = \tau_{p,y} = 500$ ps and $p_{z,\text{targ}} = 1101.3$ kPa with $\tau_{p,z} = 5$ ps). At the end of this calculation we removed the atomic velocities again. The following longer simulation (10,000 time steps) with the same parameterization was followed by one with $p_{x,\text{targ}} = p_{y,\text{targ}} = 101.3$ kPa with $\tau_{p,x} = \tau_{p,y} = 50$ ps and $p_{z,\text{targ}} = 601.3$ kPa with $\tau_{p,z} = 5$ ps. Finally an equilibration of 2.2 ns followed with equal parameters for all directions ($p_{x,\text{targ}} = p_{y,\text{targ}} = p_{z,\text{targ}} = 101.3$ kPa with $\tau_{p,x} = \tau_{p,y} = \tau_{p,z} = 0.5$ ps).

#### 3.2.5. Inserting small molecules in the membrane system

The solutes have been inserted into the equilibrated membrane box using a slow growth type procedure. In order to obtain a starting configuration for the simulations with solutes within the membrane, five heptane molecules were equally distributed in the $xy$ plane in the middle of the membrane and oriented perpendicular to the $z$-axis. For the simulations with the solute molecules outside the membrane and for the non-equilibrium simulations two heptane molecules have been inserted correspondingly in the middle of the water phase.

The insertion procedure was always the same. We performed a series of consecutive simulations at constant temperature and constant volume which had the following simulation parameters in common: a cutoff of 0.8 nm, a neighbor list cutoff of 1.0 nm, which was updated every 15 time steps, and parameters for the Berendsen thermostat, $T_{\text{targ}} = 325$ K and $\tau_T = 0.2$ ps. During a total simulation time of 110 ps with increasing simulation time step from 0.2 to 2 fs, the non-bonded interactions (Lennard–Jones and Coulomb interactions) of the solutes were stepwise increased from zero to their full values reported in Table 1. This growth period was followed by another equilibration simulation of 8 ns.

Preliminary studies showed that sulfur mustard molecules have the tendency to aggregate with each other within the membrane—an effect which is beyond the scope of this work. Therefore, we reduced the number of solutes using the procedure described above to obtain systems with only one molecule for the sulfur mustard equilibrium simulations and with two molecules for all non-equilibrium simulations.

The insertion/growth procedure described above has always been performed with the heptane molecules. To generate starting configurations for systems containing sulfur mustard, we just changed the LJ parameters and partial charges of the corresponding heptane simulation into the ones of sulfur mustard. Then, keeping the same simulation setup as described above, another equilibration of 300,000 time steps (6 ns) was performed for this system.

The production runs used the parameterization already shown: $r_{\text{cutoff}} = 0.8$ nm, a neighbor list updated every 15 time steps with a cutoff of 1.0 nm, $T_{\text{targ}} = 325$ K, $\tau_T = 0.2$ ps, $p_{\text{targ}} = 101.3$ kPa, $\tau_p = 0.5$ ps, and a time step of 2 fs. For evaluation purpose the coordinates and velocities were written into a trajectory file every 1000 time steps.

#### 3.2.6. Equilibrium simulations of sulfur mustard and heptane in the DPPC bilayer system

The four different systems (sulfur mustard and heptane each in the water phase and in the tail region of the DPPC system) were simulated with the same parameters: cutoff radius $r_{\text{cutoff}} = 1.2$ nm with a reaction field dielectric $\varepsilon = 54$, neighbor list cutoff 1.4 nm (updated every 15 time steps), $T_{\text{targ}} = 325$ K with $\tau_T = 0.2$ ps, diagonal pressure control ($\kappa_x = \kappa_y = \kappa_z = 2.77 \times 10^{-7}$ kPa$^{-1}$ and $p_{x,\text{targ}} = p_{y,\text{targ}} = p_{z,\text{targ}} = 101.3$ kPa with $\tau_{p,x} = \tau_{p,y} = \tau_{p,z} = 0.5$ ps), and a time step of 2 fs. Results and trajectories were written into files every 1000 time steps.

#### 3.2.7. Non-equilibrium simulations of sulfur mustard and heptane in the DPPC bilayer

The non-equilibrium simulations were performed with the same simulation parameters as employed in the corresponding equilibrium simulations. As starting configurations, we used the output of the simulations with two molecules of sulfur mustard or heptane in the water phase of the DPPC system. In addition to the system parameters mentioned above we applied in each time step an external force in the $+z$ direction to one of the two solute molecules and in the $-z$ direction to the other. The symmetrical force is necessary to prevent a net drift of the system. The total force on each molecule was distributed equally among all its atoms.

With both systems we ran simulations at total external forces (per one molecule) of 10, 20, 30, 50, 100, 120, 150 and 200 kJ mol$^{-1}$ nm$^{-1}$ (equal to 16.6, 33.2, 49.8, 83.0, 166.1, 199.3, 249.1, 332.1 pN). Generally, these simulations were performed for a total simulation time of at least 20 ns. Exceptions as well as the exact simulation times are reported in Section 4.

To check the influence of charges and size of the atoms, we also simulated two hypothetical molecules: a molecule of sulfur mustard constrained to have a polarity identical to that of heptane (zero partial charges), and a molecule of heptane constrained to have a polarity identical to that of sulfur mustard. With each of these parameterizations we performed simulations with a total external force per molecule of 10, 50, 100 and 200 kJ mol$^{-1}$ nm$^{-1}$.

## 4. Results and discussion

### 4.1. Characterization of the membrane system

In Fig. 2 a density profile of the DPPC membrane in equilibrium without any solute is displayed. We also show the partial densities of specific atom types. Depending on the application of different criteria, the membrane thickness $d_{\text{mem}}$ differs. The average distance between the density peaks yields a membrane thickness of

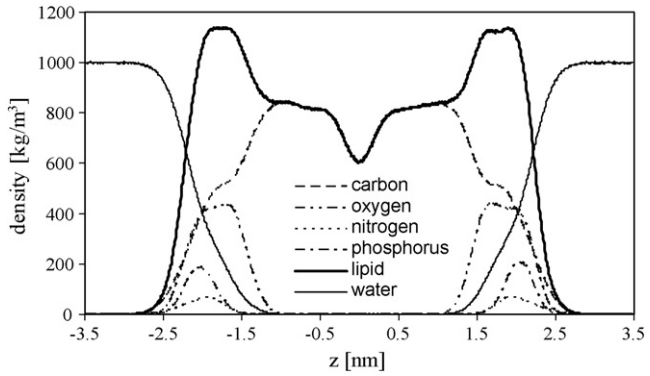


**Fig. 2.** Characterizing the membrane: density profiles of different atom types. On the basis of these profiles different membrane thicknesses $d$ can be defined: $d = 4.43$ nm between the points of equal densities of water and lipid, $d = 4.079$ nm between the maxima of the phosphorus position.

**Table 3**
Calculated tracer diffusion coefficients $D$ of the molecules in equilibrium simulations.

| System and temperature | $D$ (heptane) [$10^{-6}$ cm$^2$/s] | $D$ (sulfur mustard) [$10^{-6}$ cm$^2$/s] | $D$ (water) [$10^{-6}$ cm$^2$/s] | $D$ (DPPC in bilayer)[a] [$10^{-6}$ cm$^2$/s] |
|---|---|---|---|---|
| Pure system, 300 K | 17.2 ± 0.6 | 15.9 ± 1.0 | 23.6 ± 1.2 | – |
| Solute in water, 300 K | 18.5 ± 3.4 | 18.7 ± 2.7 | 23.6 ± 1.2 | – |
| Pure system, 325 K | 24.7 ± 2.3 | 21.4 ± 2.1 | 35.5 ± 2.1 | 0.179 ± 0.017 |
| Solute in bilayer, 325 K | 0.135 ± 0.005 | 2.15 ± 0.63 | – | – |

[a] Lateral diffusion, only in 2 dimensions.

$d_{mem}$ = 3.771 nm, the difference of the phosphorus maxima leads to $d_{mem}$ = 4.079 nm, and the one of nitrogen to $d$ = 3.69 nm. All these lengths are comparable to experimentally measured thicknesses: either $d_{mem}$ = 3.6 nm using atomic force microscopy (AFM) cross section at 50 °C by Leonenko et al. [33] or $d_{mem}$ = 3.87 nm using X-ray diffraction by Tristam-Nagle et al. [34].

Another benchmark to test the lipid force field is the area per head-group $A$ which is obtained by dividing the area of the $xy$ plane (with box lengths $L_x$ and $L_y$) by the number of lipids in a monolayer:

$$A = \frac{L_x L_y}{64}. \quad (7)$$

As Nagle and Tristram-Nagle show in their review article about membranes [35] the values measured for this property vary substantially. On the basis of that paper the authors of the GROMOS lipid force field [16], which we adopted, optimized their parameters for an area per lipid of $A$ = 0.61 nm$^2$ (reported results range from $A$ = 0.57 to 0.64 nm$^2$). We observed an area per head group for this force field between 0.59 and 0.60 nm$^2$. We consider this a sufficient agreement with the original force field, since the two calculations differ not only in the treatment of torsions but also in charge groups (which we do not use). The consequence of the smaller area per head-group is a denser system, which has to be penetrated by the solutes.

Since the motions of the solutes also depend on the motion of the environment, the diffusion constant of the lipid is the last benchmark to compare to the literature. The lateral diffusion in the $x$ and the $y$ direction only (in Eq. (4) the dimension is dim = 2) leads to a calculated diffusion coefficient of $D_{lat} = (1.79 \pm 0.17) \times 10^{-8}$ cm$^2$/s. This can be compared to the diffusion coefficient $D_{lat} = 1 \times 10^{-8}$ cm$^2$/s measured by quasi-elastic neutron scattering (QENS) at $T$ = 333 K [36,37] and $D_{lat} = 1.3 \times 10^{-8}$ cm$^2$/s measured by fluorescence recovery after photobleaching (FRAP) [38] at $T$ = 323 K. Thus, although the density in the system is in the upper part of the reported values, the diffusion of the lipids is in the right order, but marginally faster.

### 4.2. Characterization of the solute molecules

For the pure heptane system equilibrium simulations at 300 and at 325 K lead to system densities of 718 ± 2 and 703 ± 2 kg/m$^3$. These densities are 6–7% larger than the experimental ones (0.67955 kg/m$^3$ at 298.15 K [39]) and therefore considered good enough for the following comparison. The diffusion coefficients of this and all other equilibrium systems are summarized in Table 3. The mean square displacements leading to these results are plotted in Fig. 3. For pure heptane, increasing the temperature by 25 K leads to an increase of the diffusion coefficient by more than 40%. A correlation of the end-to-end distance at 300 K leads to a correlation time $\tau_{ee}$(heptane) of less than 1 ps and the analysis of the angle with the $z$ axis, which in this case is an arbitrary axis, yields a correlation time $\tau_{angle}$(heptane) = 36 ps.

The dynamical properties have also been calculated for a single heptane molecule in water (the error bars, all error bars in this article are standard deviations, for the solutes in water are bigger due to poorer statistics). The diffusion coefficients of neat heptane and heptane in water are the same within the error bars. The distribution of the end-to-end distances shows a pronounced peak at 0.74 nm, it relaxes with a correlation time of $\tau_{ee}$(heptane in water) of less than 1 ps. The uncorrected angle to $z$ axis profile shows the typical cosine shape of a fully sampled spherical property projected onto an axis; the corresponding correlation time is $\tau_{angle}$(heptane in water) = 30 ps, indicating a slightly faster rotation in water than in the pure heptane system.

The simulation of pure sulfur mustard leads to a density of $\rho = (1383 \pm 3)$ kg/m$^3$ at 300 K and $\rho = (1340 \pm 2)$ kg/m$^3$ at 325 K. Compared to the density $\rho$ = 1270 kg/m$^3$ at $T$ = 298.15 K reported in the literature [4,40] the simulated system is 9% denser. The deviation of these results of this force field from the experimental value is of the same size and in the same direction as the ones for the membrane and heptane. Comparing the force field parameters for bond lengths and bond angles to results of ab initio calculations by Glukhovtsev et al. [41] we find the force field bond lengths up to 1.5% longer than the ab initio ones and the angle at the sulfur atom is bigger by 0.9% in the force field. But the thus expected lower density is overcompensated by the force field parameters for the charges and the Lennard–Jones parameters $\varepsilon$ and $\sigma$.

The dynamical properties of the model were again tested with the diffusion coefficient (Table 3) which is about 10% smaller than that of heptane. The end-to-end distance correlation times $\tau_{ee}$(sulfur mustard), which is 3 ps at 300 K and at 2 ps at 325 K and the axis to angle correlation time $\tau_{angle}$(sulfur mustard) = 17 ps at 300 K supports the interpretation that sulfur mustard is a much more flexible molecule compared to heptane.

The higher flexibility of sulfur mustard in comparison to the one of heptane can also be explained by the choice of the force field parameters. In agreement with ab initio calculation of Butterfloss and Hermans [42] and the force field parameterization procedure of Wolfe et al. [43] we set the torsion barrier around the C–S bonds in the middle of the sulfur mustard molecule lower than the torsion barrier around the corresponding C–C bond in heptane. Less torsion restriction for sulfur mustard does not only lead to faster rotation around the central bonds than in heptane but also to a larger range of (non-equilibrium) conformations it can adopt.

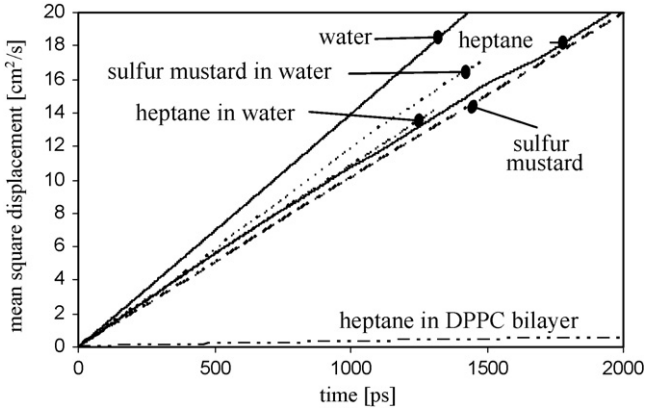


**Fig. 3.** The mean square displacements of selected molecules in different environments. In this resolution the graphs for heptane in DPPC bilayer, sulfur mustard in DPPC bilayer and the bilayer itself fall on top of each other.

Like in the heptane case, putting one sulfur mustard molecule into water shifts the diffusion coefficient towards the one of water. Within error bars it is still the same as for heptane in water. The correlation times at 300 K on the other hand hint a slowing down of the internal dynamics $\tau_{ee}$(sulfur mustard in water) = 9 ps but also on a speed up of the rotational dynamics $\tau_{angle}$(sulfur mustard) = 12 ps compared to the heptane case. The similar diffusion coefficient in spite of longer internal correlations indicates that the diffusion is mainly determined by water. Under the given accuracy, differences in the force field parameterization between the molecules do not have any significant influence on the diffusion coefficients.

### 4.3. Equilibrium behavior of the solutes in the membrane

When the solutes are inserted into the membrane, their available space gets confined. In this section, we compare the distributions (averaged, static properties) and the corresponding correlation times (dynamic properties) of the average $z$ position within the membrane of the solute's central atom. Furthermore, we analyze the end-to-end distance of the solute and the angle of the end-to-end vector with the membrane normal ($z$ axis) of sulfur mustard and heptane.

Fig. 4 shows the distribution of the $z$ position of sulfur mustard molecules, defined by the central sulfur atoms, within the membrane. While in the case of only one solute the molecule samples the whole width of the membrane's tail region in the simulation time of 12 ns, this is not realized for five molecules. Here one can observe the effect on the distribution of the clustering of two molecules in the middle of the membrane. The fact that two molecules cluster for more then 2 ns in the middle of the membrane broadens the peaks in the center of the plot. To avoid such clustering effects we

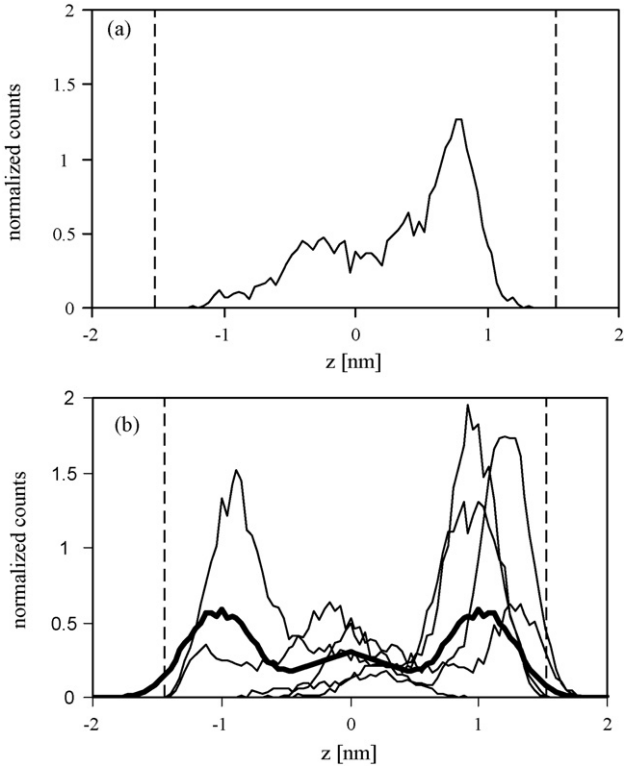


**Fig. 4.** Distribution of the central sulfur atom of one (in plot a) and five (in plot b) sulfur mustard molecules during simulations of 12 ns (plot a) and 19 ns (plot b). The vertical dashed lines indicate the average position of the innermost phosphorus atom. The thick line in the second plot is the average of the five atoms and of the two monolayers.

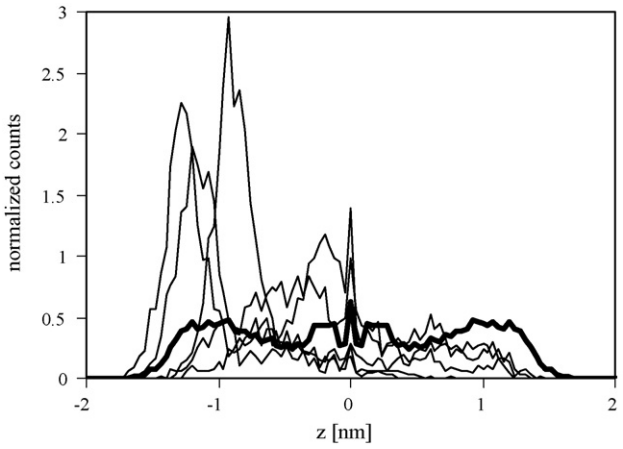


**Fig. 5.** Distribution on the central $CH_2$ groups of five heptane molecules during a simulation of 40 ns. The thick line is the average of the five heptane molecules.

continued the sulfur mustard observation with only one molecule accepting the loss of statistics. The $z$ position distribution is broad with a preferred residence in the middle of the tail region. There is, however, also a significant probability to find the molecule in the center of the membrane where the tails from opposite layers touch.

For heptane (Fig. 5), no clustering was observed. But the $z$ position distributions of the alkane molecules show other special features. First, during at least 65% of the simulation time of 40 ns, three of the five inserted molecules kept their average positions in the tail region, but nearer to the head group region than sulfur mustard. This leads to the three pronounced peaks on the left side of the profile. The other two, faster moving, molecules with broader distributions stay closer to the center of the membrane. For both we identify a pronounced sharp peak exactly in the middle of the membrane which comes from the molecules staying at the tail–tail interface for up to 10 ns.

The orientation along the $z$ axis is measured by the angle between that axis and the end-to-end vector of the solute. Division of the raw distribution by the sine of the angle removes the metric-tensor bias and leads to the graphs in Fig. 6. For sulfur mustard, we see maxima near 0° and 180° corresponding to a parallel and an anti-parallel orientation to the $z$-axis. Although the most favorable orientation is an alignment with the lipid tails, there is still a count of one sixth of the maximum for orientations perpendicular to the $z$-axis.

In comparison, the heptane molecules exhibit a more confined orientation distribution. They show even more alignment than sulfur mustard molecules, and the amount of parallelly oriented molecules is lower. We note, not shown, that there is also a reduced rotational mobility: Two of the five molecules even do not change the net orientation (cross the 90° mark) at all. These facts indicate that the heptane molecules are caged between the lipid tails with only little space to wiggle around. Both their compatibility with the lipid tails and their larger inherent stiffness (as compared to sulfur mustard) might contribute to the reduced reorientation dynamics.

In Fig. 7 we combine the information of the position of a solute and its orientation into a contour plot. Both molecules are similar in that their intensity maxima are in the corners of the diagram, i.e. the most likely situation is the molecule being embedded among the lipid tails and oriented parallel to them. There are, however, important differences. In the sulfur mustard diagram there is a straight horizontal path connecting the two maxima at constant $z$ = 0.75 nm. This means that sulfur mustard molecules can rotate in place while remaining in the lipid tail region. For heptane, there is

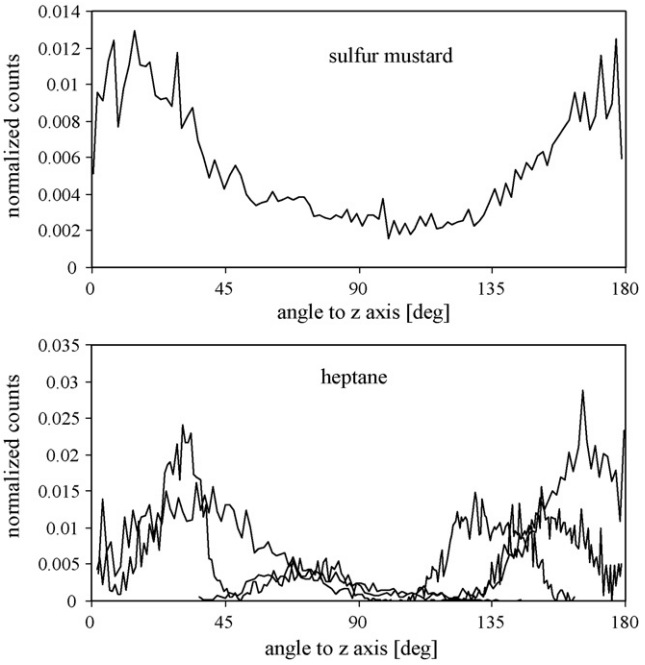


**Fig. 6.** Orientation of the inserted molecules within the membrane: The orientation of the sulfur mustard molecules (upper figure) over 12 ns show an equilibrated behavior, sampling the orientation parallel and anti-parallel to the $z$ axis with equivalent weight. In contrast the heptane molecules show a very limited sampling of the rotational space over the simulation time of 40 ns. Three molecules even did not change the sign of their orientation with respect to the $z$ axis.

a much stronger dependence between orientation and position. A heptane molecule can really only (reluctantly) adopt a perpendicular orientation at the membrane center, where opposite lipid tails touch and where the density is lower (cf. Fig. 1). A possible explanation is the lower stiffness of sulfur mustard, which would allow the molecules to reorient via an intermediate folded state, whereas the heptane molecule must rotate in a straight, extended configuration and therefore requires more free volume.

### 4.4. Non-equilibrium simulations of forced permeation by the solutes

The application of an external force drags the two sulfur mustard or heptane molecules through the system. In Fig. 8 we visualized

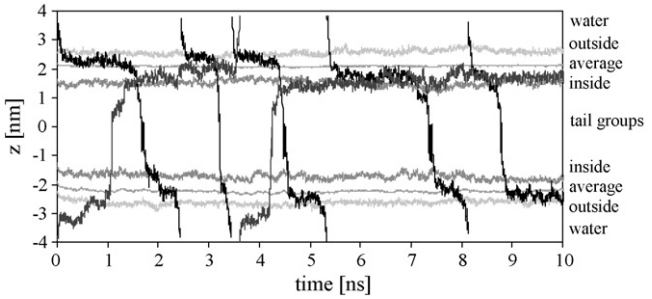


**Fig. 8.** Tracking the position of sulfur mustard molecules (sulfur atom). This example was taken from the simulation with an external force of 50 kJ mol$^{-1}$ nm$^{-1}$. The black lines show the $z$ coordinate of the central sulfur atom. The grey lines correspond to the $z$ positions of specific head groups measured by the position of the phosphorus atoms; i.e. the position of the head group most exposed to the water phase (bright grey), the average position of all head groups (grey), and the $z$ position of the innermost head group of the membrane (dark grey).

this dragging process for an external force of 50 kJ mol$^{-1}$ nm$^{-1}$ (83 pN) applied to one sulfur mustard molecule in the $+z$ direction (upwards) and the same force on the other sulfur mustard molecule in the $-z$ direction (downwards). We also introduce four different spatial regions important for the following discussion. The water region is the space between the outermost (the most exposed to the water region) phosphorus atoms of the two monolayers (recall that the box is periodic). The tail region is the space between the innermost phosphorus atoms of the two monolayers. The two head group areas are defined as the space between the outermost and the innermost phosphorus atoms of the same monolayer. These two regions are treated separately. The head-in group refers to the head group through which the solute penetrates form the water region into the tail region. The head-out group is the head group through which the solute leaves the membrane and diffuses into the water region.

For the calculation of cycles and residence times, sampling starts at the moment when the solute crosses the first region interface and ends when the solute crosses a region interface for the last time in that simulation run. This choice allowed us to take into account only completely traversed regions.

We tried several drag forces between 10 and 200 kJ mol$^{-1}$ nm$^{-1}$. For heptane simulations up to and including an external force of 30 kJ mol$^{-1}$ nm$^{-1}$, we did not observe any region crossing events. For sulfur mustard, however, we have seen at least one crossing between regions during each simulation, even for

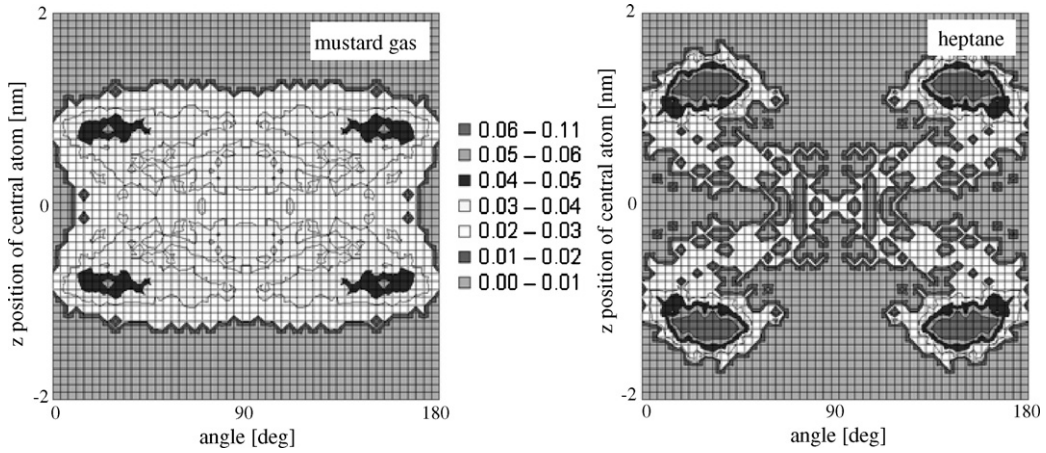


**Fig. 7.** Correlation of the orientation and the position in $z$ direction of the solutes. In case of sulfur mustard, the solute travels across the whole membrane and may have any orientation at any position in the membrane. The average position peaks of heptane molecules, which keep their $z$ position for a much longer time than the sulfur mustard, are very pronounced. And there is a clear path obvious under which circumstances the molecule is allowed to change its orientation.

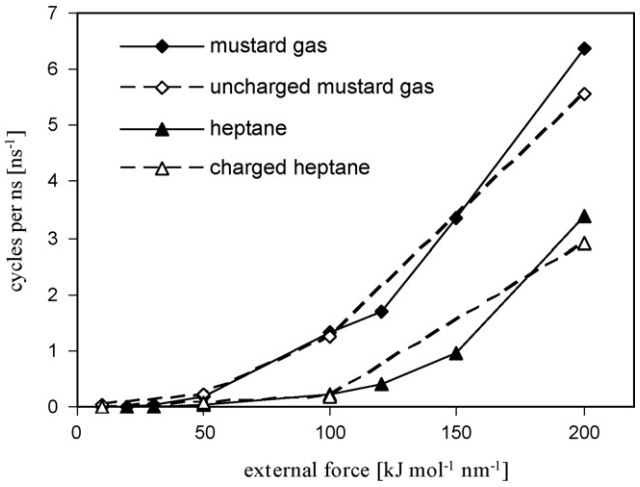


**Fig. 9.** Number of membrane penetration cycles per one sulfur mustard molecule (squares) or one heptane molecule (triangles) during 1 ns as a function of the external force acting on the molecules. While at forces smaller than the threshold of 50 kJ mol$^{-1}$ nm$^{-1}$ no complete membrane penetration was traceable, the molecules started to break through the membrane at higher external forces. Sulfur mustard is the faster of the two molecules. Also included are unphysically modified molecules in which the patterns of partial charges have been modified.

$F$ = 10 kJ mol$^{-1}$ nm$^{-1}$. Increasing the external force, a full cycle (a molecule traversing the entire $z$ dimension of the box and arriving at the periodic image of region border it crossed first) was first observed for sulfur mustard at 30 kJ mol$^{-1}$ nm$^{-1}$. Both sulfur mustard molecules moved through all regions within the total simulation time of 23.2 ns. In the case of heptane with a larger external force of 50 kJ mol$^{-1}$ nm$^{-1}$, 1.5 cycles were obtained during a total simulation time of 28 ns.

Fig. 9 shows the permeation rate of different solutes at different external forces as the solutes average number of cycles per nanosecond. Below an external force of 50 kJ mol$^{-1}$ nm$^{-1}$ one can interpret results only qualitatively. At forces above 50 kJ mol$^{-1}$ nm$^{-1}$ sulfur mustard molecules are observed to cross the membranes at rates which are significantly higher than those of heptane. Both molecules exhibit a superlinear increase in the number of cycles as a function of the external force. The heptane curve appears to be shifted by 50 kJ mol$^{-1}$ nm$^{-1}$ to higher forces. This leads to a relative increase between the number of cycles of sulfur mustard with respect to that of heptane: about a factor of 3.7 at 50 kJ mol$^{-1}$ nm$^{-1}$, 5.9 at 100 kJ mol$^{-1}$ nm$^{-1}$, and 2.0 at 200 kJ mol$^{-1}$ nm$^{-1}$.

For the force range applied, Fig. 9 clearly shows a non-linear relation between the magnitude of the external force and the resulting permeation rate. The calculations are outside the linear-response regime, and it is not possible to reliably extrapolate them to an external force of 0, which would be the natural (equilibrium) permeation rate of the two compounds. At forces small enough to be in the linear regime, there are no transition events on the timescale of the simulation. Notwithstanding, the simulations can help to identify the solute features most important for permeation. To this end, we have introduced unphysical modifications to the two molecules. We have constructed an uncharged sulfur mustard with all partial charges set to zero and all other force field parameters unchanged, as well as a charged heptane with the heptane force field parameters augmented by the charges from the sulfur mustard force field on the corresponding positions in the chain.

Charged and uncharged molecules of the same type perform (within error bars) the same number permeation events per nanosecond. Only for the strongest applied external force of 200 kJ mol$^{-1}$ nm$^{-1}$ we can see differences in the percent region between the charged and the uncharged molecules. Since except the atomic partial charges all parameters are the same and the charge is of minor importance, the different permeation rates of heptane and sulfur mustard are explained by density or free-volume considerations. The smaller molar volume (derived from the densities of the pure systems equilibrium simulations) of sulfur mustard (114 cm$^3$/mol for our model compared to 139 cm$^3$/mol for our heptane model, both at 300 K) leads to a faster penetration of the membrane.

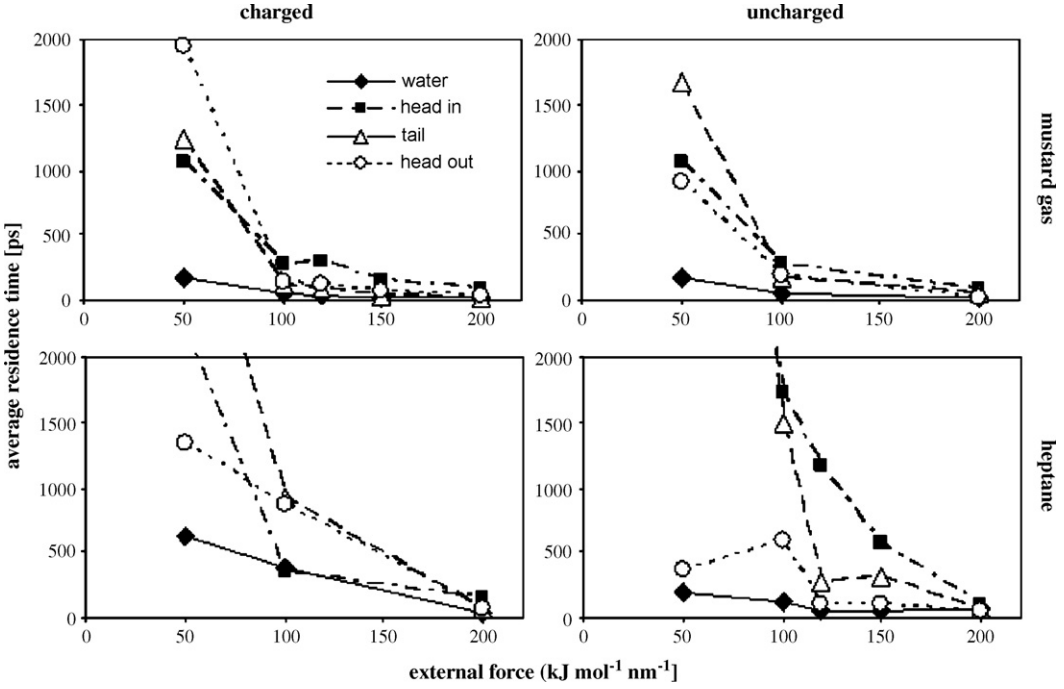


**Fig. 10.** Residence time of the solute molecules within the different compartments of the bilayer. The overall shorter residence times of sulfur mustard compared to the ones of heptane match with the general picture of more cycles per nanosecond, when an external force is applied. The unphysical solutes show that the partial charges on the beads help to penetrate the head group area.

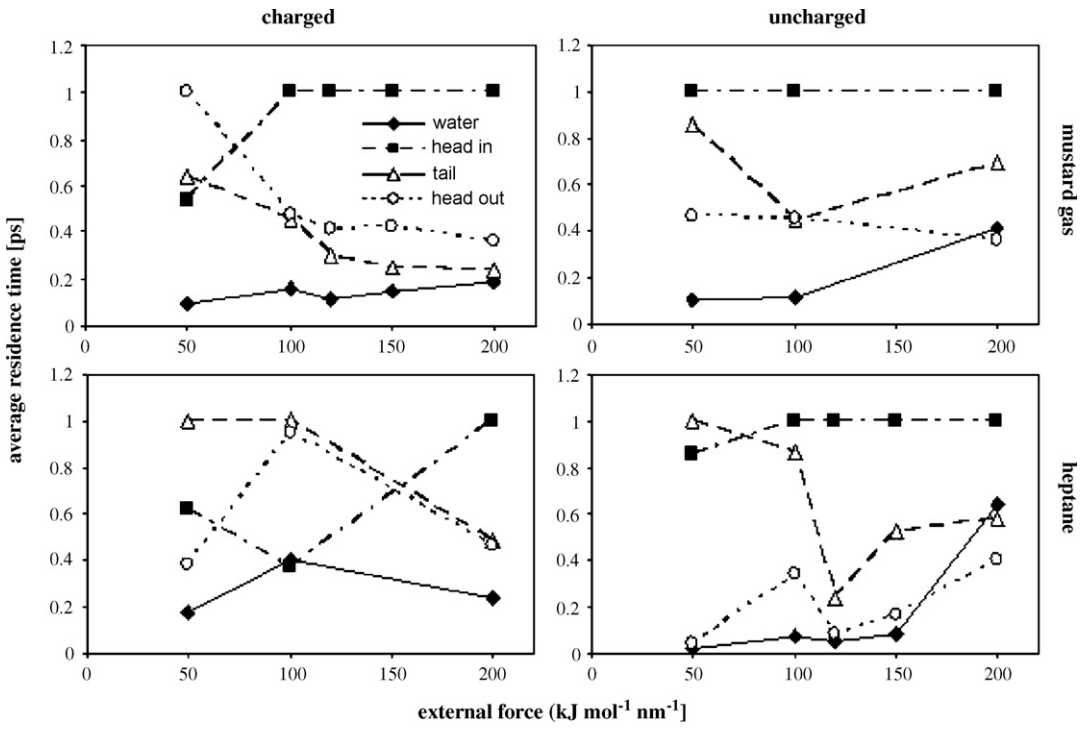


**Fig. 11.** Relative residence times of different solutes in the different regions of the membrane. The times are scaled so that the longest residence time becomes 1.

The average residence time of different molecules in the four regions of the membrane is shown in Fig. 10. Note that especially for the data at 50 kJ mol$^{-1}$ nm$^{-1}$ the statistics are limited. The shortest residence times of the solutes in all simulations are found in the water region, with its average thickness of $d_{water}$ = 1.67 nm. The residence times for all solutes are comparable, except for the charged heptane where they are approximately twice as big.

With different external forces, different regions become more important as obstacles for the solutes. Fig. 11 shows this in more detail. For each value of the external force, the longest residence time of all regions was normalized to 1 and all other residence times were scaled with the same factor. As we already observed in Fig. 10, the influence of the water phase is the weakest one but in the limit of high forces we find a relative increase of the importance of this region.

In these plots the importance of finding a way into the membrane, to penetrate the first head group (the "head-in" region with an average thickness of $d_{head\text{-}in}$ = 1.23 nm denotes the head-group region encountered by a solute entering the membrane from the water phase) becomes apparent, especially at big external forces. At small external forces the influence of other regions may take over. We can also see that this loss of importance of the head-in region is more pronounced for charged molecules than for the uncharged ones.

The most important observation lies in the comparison of the influence of the tail ($d_{tail}$ = 2.86 nm) and the head-out region ($d_{head\text{-}out} = d_{head\text{-}in}$ = 1.23 nm), i.e. the head group region encountered when the solute leaves the membrane. Both residence times keep their relative order for all external forces in each subplot. For most molecules the tail region is always a stronger impediment to permeation than the head-out region. The exception is real, charged mustard for which the opposite is true. These molecules need more time to leave the membrane than to travel through its tail region. This coincides with the results of the equilibrium simulations which also indicated a higher mobility of the sulfur mustard within the membrane.

As an estimate for the diffusion coefficients perpendicular to the membrane $D_{zz}$ in the different regions, we apply Eqs. (2) and (3) to runs with the best statistics, namely the runs with an external force of 200 kJ mol$^{-1}$ nm$^{-1}$. For heptane we calculate $D_{zz}$(water) = 2.91 × 10$^{-6}$ cm$^2$/s, $D_{zz}$(head-in) = 1.39 × 10$^{-6}$ cm$^2$/s, $D_{zz}$(tail) = 5.49 × 10$^{-6}$ cm$^2$/s, and $D_{zz}$(head-out) = 3.48 × 10$^{-6}$ cm$^2$/s. For sulfur mustard the diffusion coefficients across the membrane regions are: $D_{zz}$(water) = 9.81 × 10$^{-6}$ cm$^2$/s, $D_{zz}$(head-in) = 2.11 × 10$^{-6}$ cm$^2$/s, $D_{zz}$(tail) = 1.58 × 10$^{-5}$ cm$^2$/s, and $D_{zz}$(head-out) = 5.40 × 10$^{-6}$ cm$^2$/s. The comparison of the diffusion coefficients of the molecules in water with the values obtained in equilibrium simulations (cf. Table 3) shows that the diffusion constant in the non-equilibrium simulations is smaller by a factor of 2 for sulfur mustard and 6.5 for heptane. Given that this estimation is based on equations for homogeneous systems, the agreement of the results is satisfactory. Three possible explanations can be found for the deviations in the diffusion coefficients. First, the inhomogeneity of the system through which the molecules have to travel causes regions of fast and slow diffusion. Especially when escaping from a region with slow diffusion, the molecule will take some time to reach the new net drift velocity in the new environment. This is a finite-size effect. Second, the distribution of the times required to penetrate a region is not symmetric. In simulations with high external forces the different penetration times of the many penetration cycles lead to a pronounced penetration time distribution. We observed in this distribution a long tail for longer penetration times and a short one for shorter penetration times (not shown here). This would be compatible with an approximate Poisson distribution of the residence times. The average residence time therefore tends to overestimate the most probable residence time. Both problems, which have a tendency to underestimate the diffusion constant, are expected to lose influence with decreasing external forces—for the price of poorer statistics. Third, it has to be kept in mind that, while a "diffusion coefficient" can be defined and calculated as a ratio of particle flux and external force, we are

deep in the non-linear-response regime and the apparent diffusion coefficient can depend on the external force, see the discussion above.

The estimated diffusion coefficients nevertheless allow some insight in the transport of the solutes. We observe for both heptane and sulfur mustard a faster diffusion through the tail region (along the $z$ axis) than in the $xy$ plane. Even the penetration into the membrane at this external force shows a higher diffusion coefficient than the lateral diffusion coefficients of the solutes within the membrane. These numbers indicate again that the penetration processes at such extremely high external forces are fundamentally different from those at smaller or even vanishing external forces.

## 5. Conclusions

We demonstrated differences in the motion patterns of sulfur mustard and heptane molecules as they diffuse within and through DPPC bilayers. We showed that the way of penetration of the membrane by solutes must be different for the different molecules and at different external forces.

Sulfur mustard was observed to be the more flexible of the two species. It diffuses and reorients faster than heptane in the tail region of the membrane. Although the tail groups dictate the main orientation of both molecules their influence is smaller for sulfur mustard. This is also mirrored by the fact that, under an external driving force, the residence time of sulfur mustard in the tail region is shorter than the time the molecule needs to escape from the membrane through the head group region. The dynamical characteristics of sulfur mustard are due to a concerted effect of the partial charges and the smaller molecular volume. Only one of the two effects is not enough to reverse the order of the residence times as it is observed for heptane. For all these reasons we deduce that the obstacle to mustard penetration through a DPPC membrane is the head-group region encountered upon trying to leave the membrane into the water phase.

The behavior of heptane is different in many ways. It is much more confined by the tail groups while within the membrane. Its orientation is restrained and the diffusion is restricted by the cage formed by the lipid tails. This effect is so strong that even when an external force drags the molecule through the membrane, the residence time in the tail region dominates the one in the exit head-group region. This behavior is opposite of what is found for sulfur mustard. This observation is in agreement with the fact that heptane is soluble in apolar solvents but not in polar media (i.e. water and the head-groups). These results suggest that the tail groups are the limiting factor for heptane to penetrate the DPPC membrane.

Even though that the solubility of sulfur mustard in water is low (0.92 g/100 g $H_2O$ at 22 °C [4]), it is still higher than that of heptane (2.7 ppm at 25 °C [44]). Our results support this general statement and show their consequences for the penetration of biological membranes.

Finally we have shown that in dragging solutes through the system by applying an external force, the barriers for the penetration process change their influence. At high forces (we tested up to 200 kJ mol$^{-1}$ nm$^{-1}$), the solutes spend the most time trying to enter the membrane through the head group region. This process entails reorientation at the surface and finding or drilling a hole to slip through the network of membrane head groups. Reducing the external forces decreases the influence of this process. When forcing the molecules to stay close to the interface, they – in the course of time – find a gap in the constantly moving head-group layer and penetrate it. This process, compared to the brute force hole drilling at high external forces, is slower in absolute values, but faster in comparison of the residence times in the different regions of the membrane.

The present simulations are a first step in understanding the penetration process of sulfur mustard. Further investigations must aim for an improvement of the sulfur mustard force field. Especially optimizing the Lennard–Jones parameters (i.e. using the simplex algorithm as demonstrated lately for another molecules containing seven atoms [45]) to achieve better agreement with the density and a reparameterization of the force constants for angles and torsions, is important to increase the accuracy of the results. Results of longer simulations at external forces of less then 50 kJ mol$^{-1}$ nm$^{-1}$ may allow an extrapolation of the residence times to even lower forces. Since membranes are a patchwork of many components, comparisons of the behavior of sulfur mustard in membranes with different lipids can show preferred layers to penetrate.

Concluding, sulfur mustard and heptane are not only different in their chemical reactivity, but also in their physicochemical properties like diffusion and rotation. While these properties are still comparable in water, they become much more different in the heterogeneous and ordered environment of a membrane. Both the molecular volume (molar volume divided by Avogadro constant) and the charge distribution of the molecules have a determining influence on the permeation rate.

## Acknowledgements

We thank Volker Weiss for many critical discussions, Michael Böhm for a not less critical reading of the manuscript and the Deutsche Forschungsgemeinschaft for financial support.

## References

[1] R.J. Duchowic, J.A. Vilensky, Mustard gas: it's pre-World War I history, J. Chem. Educ. 84 (2007) 948–994.
[2] J.C. Harris, Gassed, Arch. Gen. Psychiatry 62 (2005) 15–18.
[3] OPC Conference of the States Parties C-12/6: Report of the OPCW on the Implementation of the Convention of the Prohibition of the Development, Production, Stockpiling and Use of Chemical Weapons and on Their Destruction in 2006, Declaration under Article III.
[4] J.A.F. Comption, Military Chemical and Biological Agents: Chemical and Toxicological Properties, The Telford Press, Caldwell, New Jersey, 1987.
[5] D.W. Riegle Jr., A.M. D'Amato, "The Riegle Report, U.S. Chemical and Biological Warfare-Related Dual Use Exports to Iraq and their Possible Impact on the Health Consequences of the Gulf War", United States Senate, 103d Congress, 2d Session, 1994.
[6] J. Borak, F.R. Sidell, Agents of chemical warfare: sulfur mustard, Ann. Emerg. Med. 21 (1992) 303–308.
[7] P.K. Shukla, P.C. Mishra, S. Suhai, Reactions of DNA bases with the anticancer nitrogen mustard mechlorethamine: a quantum chemical study, Chem. Phys. Lett. 449 (2007) 323–328.
[8] S. Wellert, H. Imhof, M. Dolle, H.J. Altmann, A. Richardt, T. Hellweg, Colloid Polym. Sci. 286 (2008) 417–426.
[9] H.J.C. Berendsen, S.-J. Marrink, Molecular dynamics of water transport through membranes: water from solvent to solute, Pure Appl. Chem. 65 (1993) 2513–2520.
[10] S.-J. Marrink, H.J.C. Berendsen, Simulation of water transport through a lipid membrane, J. Phys. Chem. 98 (1994) 4155–4168.
[11] B.L. de Groot, H. Grubmüller, Water permeation across biological membranes: mechanism and dynamics of Aquaporin-1 and GlpF, Science 294 (2001) 2353–2357.
[12] Amadeu K. Sum, Roland Faller, Juan J. de Pablo, Molecular simulation study of phospholipid bilayers and insights of the interactions with disaccharides, Biophys. J. 85 (2003) 2830–2844.
[13] C.S. Pereira, P.H. Hünenberger, Interaction of the sugars trehalose, maltose and glucose with a phospholipid bilayer: a comparative molecular dynamics study, J. Phys. Chem. B 110 (2006) 15572–15581.
[14] C.S. Pereira, R.D. Lins, I. Chandrasekhar, L.C.G. Freitas, P.H. Hünenberger, Interaction of the disaccharide trehalose with a phospholipid bilayer: a molecular dynamics study, Biophys. J. 86 (2004) 2273–2285.
[15] D.P. Tieleman, M.S.P. Sansom, H.J.C. Berendsen, Alamethicin helices in a bilayer and in solution: molecular dynamics simulations, Biophys. J. 76 (1999) 40–49.
[16] M. Pickholz, L. Saiz, M.L. Klein, Concentration effects of volatile anesthetics on the properties of model membrane: a coarse grain approach, Biophys. J. 88 (2005) 1524–1534.
[17] B.W. Lee, R. Faller, A.K. Sum, I. Vattulainen, M. Patra, M. Karttunen, Structural effects of small molecules on phospholipid bilayers investigated by molecular simulations, Fluid Phase Equilib. 225 (2004) 63–68.
[18] J.L. MacCallum, D.P. Tieleman, Interactions between small molecules and lipid bilayers, Curr. Top. Memb. 60 (2008) 227–256.

[19] Y. Wang, J. Cohen, W.F. Boron, K. Schulten, E. Tajkhorshid, Exploring gas permeability of cellular membranes and membrane channels with molecular dynamics, J. Struct. Biol. 157 (2007) 534–544.
[20] F. Müller-Plathe, YASP: a molecular simulation package, Comput. Phys. Commun. 78 (1993) 77–94.
[21] K. Tarmyshov, F. Müller-Plathe, Parallelizing a molecular dynamics algorithm on a multiprocessor workstation using OpenMP, J. Chem. Inf. Model. 45 (2005) 1943–1952.
[22] F. Müller-Plathe, Reversion the perturbation in nonequilibrium molecular dynamics: an easy ways to calculate the shear viscosity of fluids, Phys. Rev. E 59 (1999) 4894–4899.
[23] M.P. Allen, D.J. Tildesley, Computer Simulation of Liquids, Clarendon, Oxford, 1987.
[24] J.-P. Ryckaert, G. Ciccotti, H.J.C. Berendsen, Numerical integration of the Cartesian equations of motion of a system with constraints: molecular dynamics of alkanes, J. Comput. Phys. 23 (1977) 327–341.
[25] H.J.C. Berendsen, J.P.M. Postma, W.F. van Gunsteren, A. DiNola, J.R. Haak, Molecular dynamics with coupling to an external bath, J. Chem. Phys. 81 (1984) 3684–3690.
[26] F. Müller-Plathe, S.C. Rogers, W.F. van Gunsteren, Gas sorbtion and transport in polybutylene: equilibrium and nonequilibrium molecular dynamics simulations, J. Chem. Phys. 98 (1993) 9895–9904.
[27] D.J. Evans, J.P. Moriss, Statistical Mechanics of Nonequilibrium Liquids, Academic Press, London, 1990.
[28] I. Chandrasekhar, M. Kastenholz, R.D. Lins, C. Oostenbrink, L.D. Schuler, D.P. Tielemann, W.F. van Gunsteren, A consistent potential energy parameter set for lipids: dipalmitoylphosphatidulcholine as a benchmark of the GROMOS96 45A3 force field, Eur. Biophys. J. 32 (2003) 67–77.
[29] W.F. van Gunsteren, S.R. Billeter, A.A. Eising, P.H. Hünenberger, P. Krüger, A.E. Mark, W.R.P. Scott, I.G. Tironi, Biomolecular Simulation: The GROMOS96 Manual and User Guide, VDF, Zürich, 1996.
[30] CRC Handbook of Chemistry and Physics, 73rd ed., CRC Press, London, 1992–1993.
[31] M.J. Frisch, G.W. Trucks, H.B. Schlegel, G.E. Scuseria, M.A. Robb, J.R. Cheeseman, J.A. Montgomery Jr., T. Vreven, K.N. Kudin, J.C. Burant, J.M. Millam, S.S. Iyengar, J. Tomasi, V. Barone, B. Mennucci, M. Cossi, G. Scalmani, N. Rega, G.A. Petersson, H. Nakatsuji, M. Hada, M. Ehara, K. Toyota, R. Fukuda, J. Hasegawa, M. Ishida, T. Nakajima, Y. Honda, O. Kitao, H. Nakai, M. Klene, X. Li, J.E. Knox, H.P. Hratchian, J.B. Cross, C. Adamo, J. Jaramillo, R. Gomperts, R.E. Stratmann, O. Yazyev, A.J. Austin, R. Cammi, C. Pomelli, J.W. Ochterski, P.Y. Ayala, K. Morokuma, G.A. Voth, P. Salvador, J.J. Dannenberg, V.G. Zakrzewski, S. Dapprich, A.D. Daniels, M.C. Strain, O. Farkas, D.K. Malick, A.D. Rabuck, K. Raghavachari, J.B. Foresman, J.V. Ortiz, Q. Cui, A.G. Baboul, S. Clifford, J. Cioslowski, B.B. Stefanov, G. Liu, A. Liashenko, P. Piskorz, I. Komaromi, R.L. Martin, D.J. Fox, T. Keith, M.A. Al-Laham, C.Y. Peng, A. Nanayakkara, M. Challacombe, P.M.W. Gill, B. Johnson, W. Chen, M.W. Wong, C. Gonzalez, J.A. Pople, Gaussian 03 Revision B. 01, Gaussian, Inc., Pittsburgh, PA, 2003.
[32] H.J.C. Berendsen, J.R. Grigera, T.P. Straatsma, The missing term in the effective pair potentials, J. Phys. Chem. 91 (1987) 6269–6271.
[33] Z.V. Leonenko, E. Finot, H. Ma, T.E.S. Dahms, D.T. Cramb, Investigation of temperature-induced phase transition in DOPC and DPPC phospholipid bilayers using temperature controlled scanning force microscopy, Biophys J. 86 (3783) (2004) 3783–3793.
[34] S. Tristram-Nagle, T. Moore, H.I. Petrache, J.F. Nagle, Specific volumes of lipids in fully hydrated bilayer dispersions, Biochim. Biophys. Acta 938 (1988) 135–142.
[35] J.F. Nagle, S. Tristram-Nagle, Structure of bilayers, Structure of lipid bilayers, Biochim. Biophys. Acta 1469 (2000) 159–195.
[36] S. König, W. Pfeiffer, T. Bayerl, D. Richter, E.J. Sackmann, Molecular dynamics of lipid bilayers studied by incoherent quasi-elastic neutron scattering, J. Phys. II France 2 (1992) 1589–1616.
[37] R. Lipowski, E. Sackmann, Structure and Dynamics of Membranes, Elsevier, Amsterdam, 1995.
[38] P.F.F. Almeida, W.L.C. Vaz, T.E. Thompson, Lateral diffusion in the liquid phases of dimyristoylphosphatidylcholine/cholesterol lipid bilayers: a free volume analysis, Biochemistry 31 (1992) 6739–6747.
[39] J. Vijande, J.J. Piñeiro, J. García, J.L. Valencia, J.L. Legido, Density and surface tension variation with temperature for heptane + 1-alkanol, J. Chem. Eng. Data 51 (2006) 1778–1782.
[40] Report on Carcinogens, 11th ed., U.S. Department of Health and Human Services, Public Health Service, National Toxicology Program, 2005.
[41] M. Glukhovtsev, R.D. Bach, C.J. Nagel, A high-level computational study of the thermochemistry and thermal decomposition of sulfur mustard (2,2′-dichlorethyl sulfide): chemical warfare agent, J. Phys. Chem. A 102 (1998) 3438–3446.
[42] G.L. Butterfoss, J. Hermans, Boltzmann-type distribution of side-chain conformation in proteins, Protein Sci. 12 (2003) 2719–2731.
[43] S. Wolfe, D.F. Weaver, K. Yang, MMPEP: development and evaluation of peptide parameters for Allinger's MMP2(85) programme, including calculations of crambin and insulin, Can. J. Chem. 66 (1988) 2687–2702.
[44] C. Tsonopoulos, Thermodynamic analysis of the mutual solubilities of normal alkanes and water, Fluid Phase Equilib. 156 (1999) 21–33.
[45] T.J. Müller, S. Roy, W. Zhao, A. Maaß, D. Reith, Economic simplex optimisation for broad range property prediction: strengths and weaknesses of an automated approach for tailoring of parameters, Fluid Phase Equilib. 274 (2008) 27–35.